

1 **Recent decrease in summer precipitation over the Iberian Peninsula**  
2 **closely links to reduction of local moisture recycling**

3 Yubo Liu<sup>1,2</sup>, Monica Garcia<sup>3,4</sup>, Chi Zhang<sup>1,5</sup>, Qihong Tang<sup>1,2\*</sup>

4

5 <sup>1</sup>Key Laboratory of Water Cycle and Related Land Surface Processes, Institute of Geographic  
6 Sciences and Natural Resources Research, Chinese Academy of Sciences, Beijing, China

7 <sup>2</sup>University of Chinese Academy of Sciences, Beijing, China

8 <sup>3</sup>Research Center for the Management of Environmental and Agricultural Risks (CEIGRAM),  
9 E.T.S. de Ingeniería Agronómica, Alimentaria y de Biosistemas, Universidad Politécnica de  
10 Madrid, Avda. Senda del Rey, 13, 28040 Madrid, Spain

11 <sup>4</sup>Sino-Danish Center for Education and Research (SDC), 8000 Aarhus C, Denmark

12 <sup>5</sup>Key Laboratory of Land Surface Pattern and Simulation, Institute of Geographic Sciences and  
13 Natural Resources Research, Chinese Academy of Sciences, Beijing, China

14

15 **\*Correspondence:** Qihong Tang (tangqh@igsnr.ac.cn)

16

17 **Abstract**

18 The inherently dry summer climate of the Iberian Peninsula (IP) is undergoing drought  
19 exacerbated by more intense warming and reduced precipitation. Although many  
20 studies have studied changes in summer climate factors, it is still unclear how the  
21 changes in moisture contribution from the sources lead to the decrease in summer  
22 precipitation. This study investigates the differences in the IP precipitationshed between  
23 1980-1997 and 1998-2019 using the Water Accounting Model-2layers with ERA5 data,  
24 and assesses the role of local moisture recycling and external moisture in reducing  
25 summer precipitation. Our findings indicate that the moisture contributions from the  
26 local IP, and from the west and the east of the precipitationshed contributed 1.7, 3.6 and  
27 1.1 mm mon<sup>-1</sup> less precipitation after 1997 than before 1997, accounting for 26 %, 57 %  
28 and 17 % of the main source supply reduction, respectively. The significant downward  
29 trend of the IP local moisture recycling closely links to the disappearance of the wet  
30 years after 1997 as well as the decrease of local contribution in the dry years. Moreover,  
31 the feedback between the weakened local moisture recycling and the drier land surface  
32 can exacerbate the local moisture scarcity and summer drought.

33

## 34 **1. Introduction**

35       The Iberian Peninsula (IP) is located in the Mediterranean basin, which is among  
36 the global “hotspots” of climate change. The IP precipitation is characterized by the  
37 diverse climatic regimes and high spatial variability as a consequence of its geographic  
38 position between the Atlantic Ocean and the Mediterranean Sea and its orographic  
39 configuration. In responding to climate change with frequent heatwaves and above-  
40 average warming, the IP is experiencing widespread decreases in precipitation,  
41 especially in summer (Brogli et al., 2019; Cramer et al., 2018; Rajczak and Schär, 2017).  
42 This reduction in summer precipitation is a major driver of water resource depletion  
43 and the evolution of drought (Lopez-Bustins and Lemus-Canovas, 2020; Páscoa et al.,  
44 2021; Teuling et al., 2013). To clarify the reason for the decrease in summer  
45 precipitation, it is necessary to explain the changes in moisture contribution from the  
46 sources, such as local moisture recycling and external sources.

47       Analysis of source supply and transportation in the hydrological cycle has become  
48 one efficient way to understand well regional precipitation. With the introduction of the  
49 concept of precipitationshed (Keys et al., 2014; Keys et al., 2011), which better reveals  
50 the contribution from upwind evaporation sources to the precipitation in downwind sink  
51 region, it is more scientific and systematic to explain the precipitation variations by  
52 using the fluctuations of moisture contribution as a precursor. Given the importance of  
53 studying the source of precipitation, that is, precipitationshed, a variety of methods have  
54 been developed and adopted, including physical isotope analysis (Bonne et al., 2014),

55 and numerical analytical models, either online methods running in parallel with climate  
56 models (Damián and Gonzalo, 2018; Stohl and James, 2004, 2005), or offline  
57 “posteriori models” (van der Ent and Savenije, 2011; van der Ent et al., 2010; van der  
58 Ent et al., 2013). Furthermore, the local moisture recycling, which describes the local  
59 precipitation-evaporation feedback relationship, has been proposed to further  
60 differentiate regional local and external contributions to the designated area. Although  
61 the mechanisms of these studies are different, they all emphasize that the constantly  
62 changing source-sink relationship of atmospheric moisture is an essential part of  
63 climate change research as global change continues.

64 Gimeno et al. (2010) comprehensively investigated the atmospheric moisture  
65 sources of the IP precipitation at different scales, and identified the tropical–subtropical  
66 North Atlantic corridor, the surrounding Mediterranean Sea and the local IP as  
67 important moisture regions. The high precipitation in the cold season is mainly  
68 dominated by westerly wind regimes. The mid-latitude atmospheric dynamics, such as  
69 the baroclinic synoptic-scale perturbations from the Atlantic and the polar jet stream,  
70 as well as the high moisture supply from an Atlantic “tropospheric river” seem to be  
71 responsible for the abundant precipitation during the cold season (Cortesi et al., 2013;  
72 Ulbrich et al., 2015; Zhu and Newell, 1998). Compared to the rainy winter, the summer  
73 with very low precipitation receives less attention. The subtropical location under the  
74 descending air extending from the North Atlantic subtropical high controls low summer  
75 precipitation over the IP, and local convective events increase the importance of local

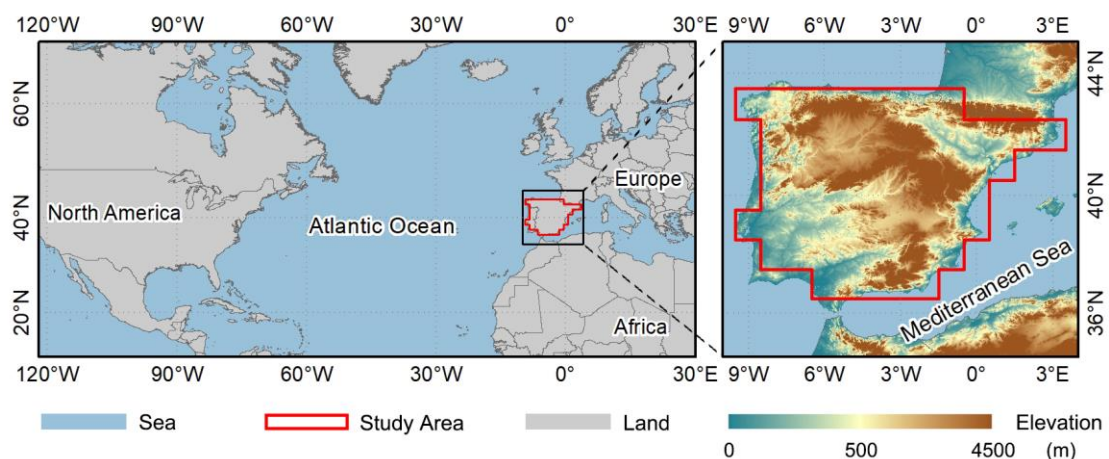
76 moisture recycling during summer (Serrano et al., 1999). Accordingly, the summer IP  
77 precipitation, with a significant proportion of the locally recycled moisture, is  
78 completely different from the winter IP precipitation that is dominated by the distant  
79 external moisture.

80 In recent decades, the increasing severity of summer drought in the IP, which is  
81 closely related to precipitation variations, has attracted more attention. Several  
82 mechanisms, including soil-atmosphere interactions (Boé and Terray, 2014), cloud  
83 processes (Lenderink et al., 2007; Tang et al., 2012) and large-scale circulation changes  
84 (Boé et al., 2009; Brogli et al., 2019; Kröner et al., 2017), have been found to be  
85 potentially important for this complex summer climate change, which also appear to  
86 have an impact on the precipitation reduction. Such anomaly of summer precipitation  
87 in the sink is inevitably linked to source changes, but there is still a lack of knowledge  
88 about how source moisture contributes to precipitation decline. Therefore, tracing the  
89 precipitationshed of the IP and quantifying the moisture contributions can provide us  
90 with a new perspective to analyze the changes in IP precipitation. This study aims to  
91 evaluate the moisture contribution of the local moisture recycling and external sources  
92 to the reduced summer precipitation over the IP. It can provide a scientific reference for  
93 the prediction and management of droughts that may be caused by precipitation  
94 reduction from the perspective of source moisture contribution.

## 95 2. Study Area, Data and Methods

### 96 2.1 Study area

97 The IP is located in southwestern Europe at midlatitudes of the northern  
98 hemisphere. It covers Portugal and the mainland of Spain. The geographic location of  
99 IP is shown in Fig. 1(a) (36°N-44°N, 10°W-3°E) in a transition zone between  
100 midlatitude and subtropical atmospheric circulation regimes. It has a complex  
101 topography, surrounded by the Atlantic Ocean and Mediterranean Sea, and elevated in  
102 the middle and northeast. The topographic and coastal processes affect water vapor  
103 transport, forming a spatial precipitation gradient from the northwest to the southeast.  
104 Extracted from the land-sea mask provided by European Centre for Medium-range  
105 Weather Forecasts (ECMWF), the red outline area composed of multiple single 1×1  
106 degree grids is our study area of the IP.



108 **Figure 1** Map of the IP (the area within the closure of the red line) on a grid of 1°×1° as the target  
109 region.

110

## 111 2.2Data

112 The newest reanalysis data held in ECMWF data archive, the ERA5 dataset  
113 downloaded from the Copernicus Climate Change Service (C3S) Climate Data Store  
114 (CDS) is used in this study (Hersbach et al., 2020). The variables include surface  
115 pressure, precipitation, evaporation, total column water, and vertical integrated  
116 eastward and northward atmospheric water fluxes (including cloud liquid water flux,  
117 cloud frozen water flux and water vapor flux) on single level, as well as the horizontal  
118 U/V components of wind fields and specific humidity at the lowest 23<sup>rd</sup> pressure levels  
119 (200-1000hPa). The time resolution and spatial resolution selected for these data are 1  
120 hour and 1×1 degree, respectively. This dataset covers the period from 1980 to 2019.  
121 Compared to the old version reanalysis data (e.g., ERA-Interim or ERA-40), ERA5  
122 combines vast amounts of historical observations into global estimates using more  
123 advanced modelling and data assimilation systems (Hersbach et al., 2020).

124 As the ERA5 precipitation is a global forecast dataset with some uncertainties, its  
125 reliability in the IP region needs to be verified. Therefore, an observational gridded  
126 dataset generated from a dense network of stations over the IP, named the Iberia01  
127 (Herrera et al., 2019), is used to verify the accuracy of the ERA5 precipitation data. The  
128 Iberia01 provides the daily precipitation for the period of 1971-2015 at 0.1×0.1 degree.

## 129 2.3 Model and methods

### 130 2.3.1 Water Accounting Model-2layers

131 Water Accounting Model-2layers (WAM-2layers) is an offline Eulerian method  
132 tracking the moisture cycle forwards or backwards that quantifies the source-sink  
133 relations (van der Ent et al., 2013; van der Ent et al., 2014). Its backward algorithm was  
134 used in this study to trace the precipitation shed of the IP. The model of WAM-2layers  
135 is an updated version of the original WAM. The water vapor balance equation in the  
136 WAM-2layers algorithm maintains the premise that the atmosphere is well mixed, but  
137 compared with the previous model, it takes the stratification of the atmosphere into  
138 consideration. Thus, when the algorithm is applied to a specific region, the calculation  
139 is as follows,

$$140 \quad \frac{\partial W_{l,r}}{\partial t} + \frac{\partial(W_{l,r}u)}{\partial x} + \frac{\partial(W_{l,r}v)}{\partial y} = E_{l,r} - P_{l,r} \pm F_{v,r} + \alpha_{l,r} \quad (1)$$

141 where  $W$  is the atmospheric moisture storage, or namely, precipitable water;  $t$  is time;  $u$   
142 and  $v$  are the wind components in  $x$  (zonal) and  $y$  (meridional) direction, respectively;  
143  $E$  is evaporation;  $P$  is precipitation;  $F_V$  is the vertical moisture transport between the  
144 bottom and top layer;  $\alpha$  is a residual term, which is resulted from the ERA5 data  
145 assimilation and the coarser resolution scheme in the model calculation (van der Ent et  
146 al., 2014); the subscript  $l$  represents the portion in layer  $l$  (either the bottom layer or the  
147 top layer), and the subscript  $r$  represents the tagged portion provided by the source  
148 region.



149 Based on the assumption of a well-mixed atmosphere (Burde, 2010; Goessling and  
 150 Reick, 2013), the moisture contribution, that is, the tagged evaporation  $E_r$ , can be  
 151 calculated considering that the ratio of tagged to total atmospheric water storage is equal  
 152 to the ratio of tagged to total evaporation, as shown in Eq. (2). Considering the proposed  
 153 retention time of atmospheric moisture is about 1 week to 10 days (Numaguti, 1999),  
 154 we set the backtracking time as 1 month longer for summer precipitation to make sure  
 155 that more than 90 % of the precipitation can be redistributed to the surface (Zhang et  
 156 al., 2017).

$$157 \quad E_r(t, x, y) = E(t, x, y) \frac{W_r(t, x, y)}{W(t, x, y)} \quad (2)$$

158 The main moisture source supplying IP summer precipitation is defined as the 90<sup>th</sup>  
 159 percentile precipitation shed in this study. It is further divided into subregions to  
 160 evaluate the role of the contribution from each area, such as the local moisture recycling,  
 161 which demonstrates the contribution of local evaporation to the IP precipitation, and  
 162 the external advection moisture, which describes the non-local evaporation contribution  
 163 to the IP precipitation. The contribution ratio ( $CR$ ) of a subregion ( $A$ ) is defined as the  
 164 proportion of the moisture contribution from it to the total contribution from the main  
 165 source region ( $MS$ ), which is calculated as the following Eq. (3). The precipitation  
 166 recycling ratio of the IP can be substituted with the IP local contribution ratio  $CR_{IP}$ .

$$167 \quad CR_A = \frac{\sum E_r(t, x, y|A)}{\sum E_r(t, x, y|MS)} \times 100\% \quad (3)$$

168 2.3.2 Significance test

169 The slope significance of trend fitting and the significance of the difference in the  
 170 means are tested using Student t-test in this study. Additionally, the ~~moving sliding~~-t-  
 171 test, as a method of mutation analysis, is used to detect whether and when the sample  
 172 mean in the IP precipitation series changed significantly. The precipitation series is  
 173 divided into two non-overlapping adjacent segments of length  $n$  years before and after  
 174 the reference year, to compare changes in the mean (Maasch, 1988),

$$175 T = \frac{\frac{1}{n_1} \sum_{t=1}^{n_1} x - \frac{1}{n_2} \sum_{t=n_1+1}^{n_1+n_2} x}{\frac{(n_1-1)S_1^2 + (n_2-1)S_2^2}{n_1+n_2-2} \sqrt{\frac{1}{n_1} + \frac{1}{n_2}}}$$

$$176 T = \frac{(\bar{x}_1 - \bar{x}_2)\sqrt{n}}{\sqrt{S_1^2 + S_2^2}} \quad (4)$$

177 where  $\bar{x}_1$  and  $\bar{x}_2$  denote the respective means of two segments,  $x$  is the precipitation  
 178 series to be tested,  $n_1$  and  $n_2$  are step lengths set for two sequences before and after the  
 179 moving point, and  $S_1^2$  and  $S_2^2$  are their variances, of the two sequences which can be  
 180 calculated as following.

$$181 S_1^2 = \frac{1}{n_1-1} \sum_{t=1}^{n_1} \left( x - \frac{1}{n_1} \sum_{t=1}^{n_1} x \right)^2 \quad (5)$$

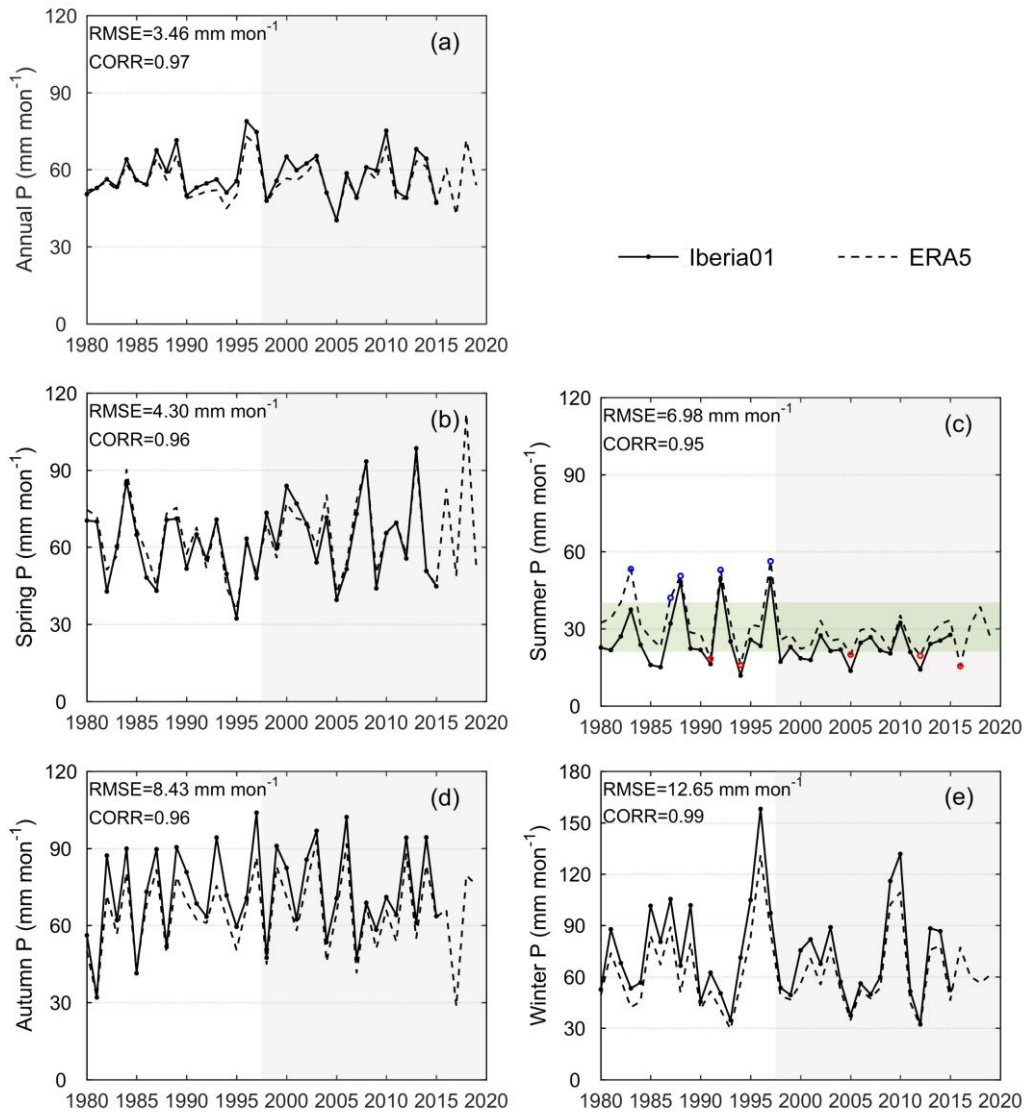
$$182 S_2^2 = \frac{1}{n_2-1} \sum_{t=n_1+1}^{n_1+n_2} \left( x - \frac{1}{n_2} \sum_{t=n_1+1}^{n_1+n_2} x \right)^2 \quad (6)$$

183 **3. Results**

184 3.1 Evaluation and variation of precipitation data

185 The precipitation time series of the ERA5 and the Iberia01 data are shown in Fig.

186 2. The fluctuations and variations of the ERA5 precipitation data are in good agreement  
187 with the observed data on both annual and seasonal scales, together with all correlation  
188 coefficients higher than 0.95. The average annual precipitation over the IP is about  
189 55.66 mm mon<sup>-1</sup> from ERA5 and 58.07 mm mon<sup>-1</sup> from Iberia01, respectively.  
190 Compared with the observed data, the reanalysis data slightly underestimates the IP  
191 precipitation with the root mean square error (RMSE) of 3.46 mm mon<sup>-1</sup> on the annual  
192 scale. The comparison of seasonal precipitation shows that the ERA5 is lower than the  
193 observed Iberia01 value in the rainy seasons (both winter and autumn), but higher in  
194 the dry summer. The RMSE between the two datasets of seasonal precipitation is in the  
195 range of 4.30-12.65 mm mon<sup>-1</sup>. Since the Iberia01 data is the grid data interpolated from  
196 observation site data (Herrera et al., 2019), some of the deviations between the ERA5  
197 and the Iberia01 precipitation can be partially affected by the interpolation process  
198 rather than solely the result of the error generated by the reanalysis process. In general,  
199 the ERA5 precipitation data shows the characteristics of IP precipitation reasonably  
200 well and thus is suitable for studying the changes.



201

202 **Figure 2** Variations of IP (a) annual precipitation, (b) spring (March, April and May), (c) summer

203 (June, July and August), (d) autumn (September, October and November) and (e) winter (December,

204 January and February) during 1980-2019. The white shading is for the period 1980-1997 and the

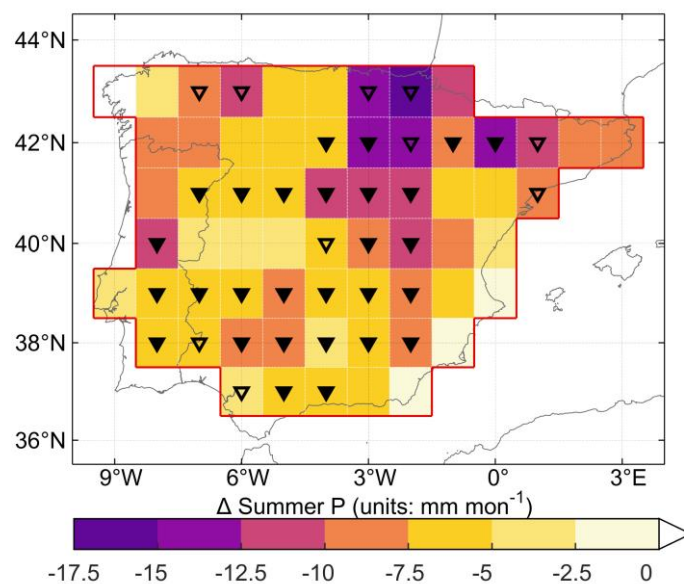
205 grey shading is for the period 1998-2019. The green shading covers the interval of one standard

206 deviation of summer precipitation. The years with summer ERA5 precipitation exceeding the range

207 of the green shading interval are circled in blue and red.

208 Only in summer, the mutation analysis results of the two sets of precipitation data,

209 the Iberia01 (T value: 1.83) and the ERA5 (T value: 1.86), both show statistically  
 210 significant changes at 0.1 level in the year 1997. Accordingly, the entire 40-year period  
 211 is divided into two periods, 1980-1997 and 1998-2019, to compare the difference in  
 212 summer precipitation between the two periods. The average summer precipitation is  
 213 34.89 and 27.17 mm mon<sup>-1</sup> before and after 1997, respectively. Compared with 1980-  
 214 1997, the average summer precipitation during 1998-2019 decreases by 7.72 mm  
 215 (22.13 %) in the whole study area. On the grid scale, almost all grids have less  
 216 precipitation after 1997, and more than half of all grids show the statistically significant  
 217 reductions (Fig. 3). However, this change is unevenly distributed in space, as shown by  
 218 the greater reduction in the grids on the northeastern IP that can even exceed 10 mm  
 219 mon<sup>-1</sup>.



220

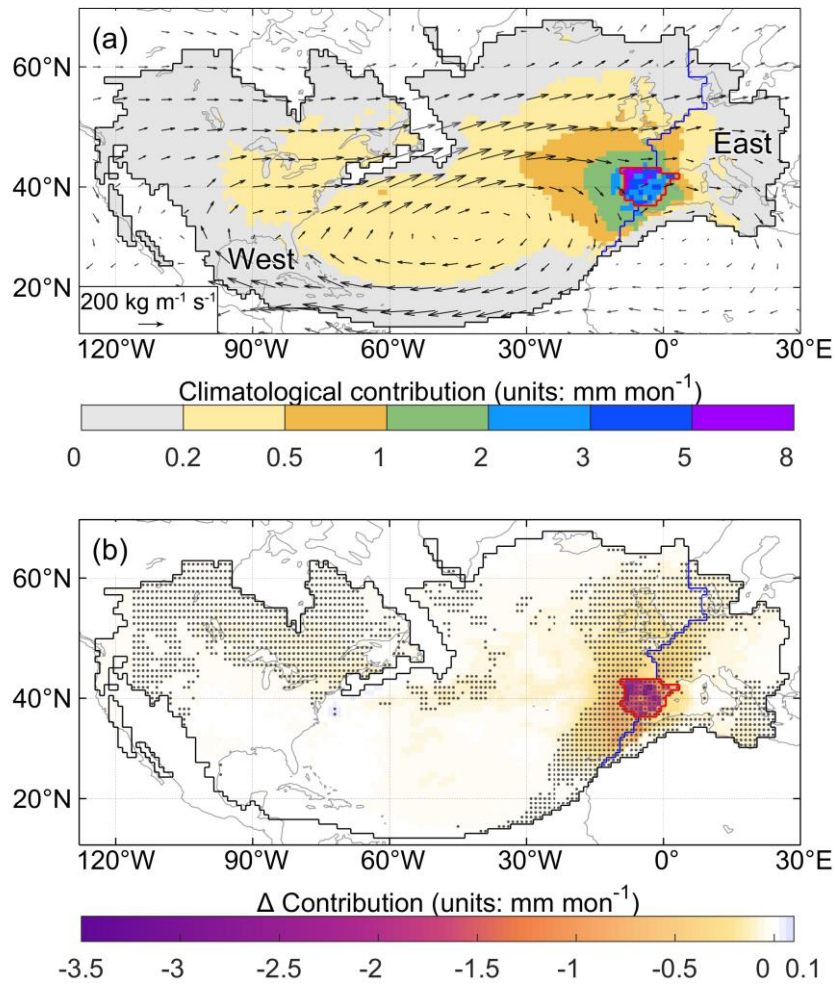
221 **Figure 3** The difference of average summer precipitation over the IP between 1998-2019 and 1980-  
222 1997 (average of 1998-2019 minus average of 1980-1997). The triangles indicate that the  
223 differences are significant at 0.05 (solid) and 0.1 (hollow) level.

224 For summer precipitation, the dry years (1991, 1994, 2005, 2012 and 2016) and  
225 the wet years (1983 1987 1988 1992 and 1997) are selected, which are circled in Fig.  
226 2(c). A wet year is defined as the year in which the precipitation is more than one  
227 standard deviation above the average precipitation, and similarly, the precipitation in a  
228 dry year is lower than a standard deviation range. Accordingly, the division of time  
229 period also applies to the precipitation series of the dry and wet years. It is specifically  
230 observed that the dry years are distributed in both two periods, with the average  
231 precipitation of 17.15 and 18.34 mm mon<sup>-1</sup> before and after 1997, whereas the wet years  
232 occur before 1997 with an average of 51.03 mm mon<sup>-1</sup> but disappear after 1997.

### 233 3.2 Changes in summer precipitation shed and regional contributions

234 From 1980 to 2019, the average value of the IP summer precipitation is about  
235 30.64 mm mon<sup>-1</sup>. More than 93 % of this summer precipitation has been tracked by the  
236 global surface through modelling, averaging 28.53 mm mon<sup>-1</sup>. The climatology of the  
237 moisture contribution during the 40 years is shown in Fig. 4(a). The moisture  
238 contribution to the IP generally decreases as its distance to IP increases. Although the  
239 precipitation shed of the IP summer precipitation is global in scope, the contribution of  
240 the area far away is negligible to be considered. Therefore, the 90<sup>th</sup> precipitation shed

241 enclosed by the black line in Fig. 4 is given full attention as the main moisture source  
242 region in the following text. The main moisture source of the IP covers not only the  
243 local grids in the study region, but also several of non-local land and oceanic areas. Due  
244 to the dominance of the westerlies in the tropical–subtropical North Atlantic corridor  
245 (Gimeno et al., 2010), most of the non-local source grids are located in the North  
246 American land and the North Atlantic Ocean west of the study area, which jointly form  
247 a relatively stable atmospheric basin in the global atmospheric moisture networks  
248 (Zhang et al., 2020) under the influence of the summer anticyclonic structure (Fig. 4(a)).  
249 The other source grids are located east of the North Atlantic Ocean and the IP, which is  
250 the downwind zone for water vapor transport, covering Western Europe and the  
251 Mediterranean. These eastern regions with positive atmospheric moisture divergence  
252 provide a net water flux to the atmosphere, moisten the air parcels flowing towards the  
253 surrounding land, and become the main short-term moisture sources affecting the IP,  
254 especially the eastern IP (Gimeno et al., 2010; Vázquez et al., 2020). Hence, the main  
255 moisture sources are divided into the three partial regions of the local IP, the west and  
256 the east by the boundary of the study area and the eastern boundary of the Atlantic  
257 Ocean (red and blue lines in Fig. 4), and the contribution of each region to the IP  
258 precipitation can be quantified and compared.



259

260 **Figure 4** (a) Climatological 90<sup>th</sup> precipitation shed of the IP sink region and moisture contribution  
 261 to the IP summer precipitation from 1980 to 2019. The black outlines show the 90<sup>th</sup> precipitation shed  
 262 boundary during the 40 years. The vectors represent the climatological monthly water vapor flux.  
 263 The red line encloses the study area, and the blue line divides the precipitation shed excluding the IP  
 264 into the west (left area) and the east (right area) regions. (b) Differences in the moisture contribution  
 265 in the 90<sup>th</sup> precipitation shed between 1998-2019 and 1980-1997 (average of 1998-2019 minus  
 266 average of 1980-1997). The dots indicate 0.1 significance of the difference.

267 Affected by the transport distance, the grids with high contribution are located in  
 268 and around the target IP region, with the maximum values for grids in the northwest

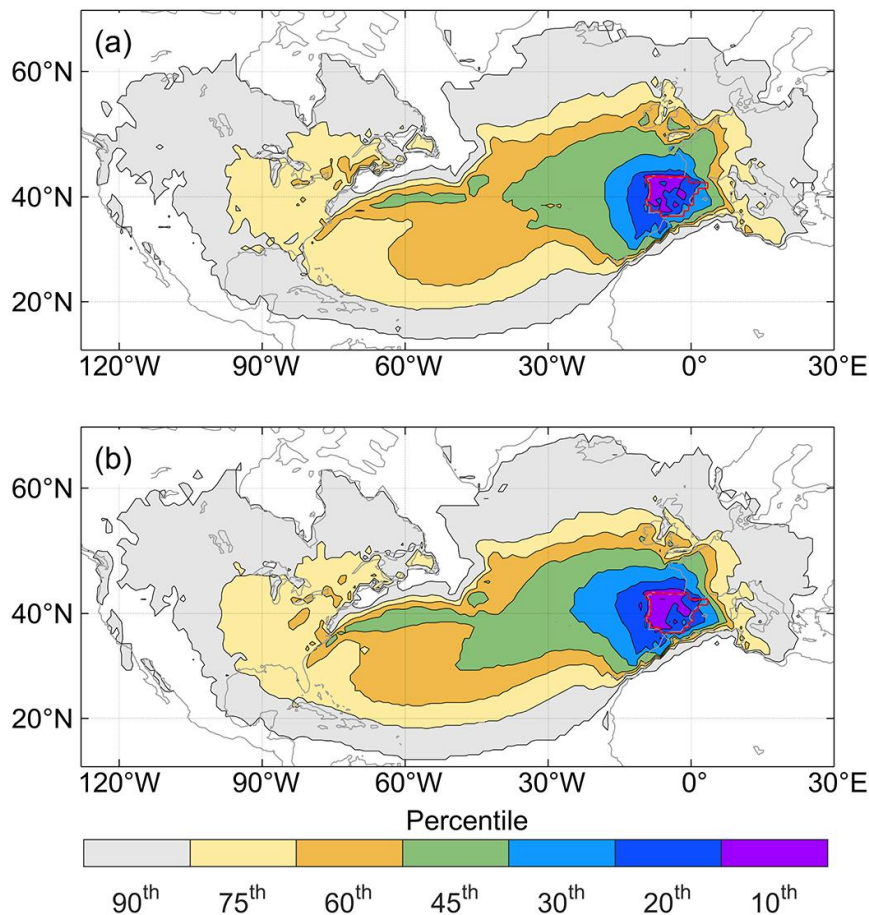


269 corner of the IP. The local IP contributes  $3.46 \text{ mm mon}^{-1}$  average summer precipitation,  
270 with the precipitation recycling ratio of around 13.26 % during the 40 years. The west,  
271 as the largest subregion of the precipitationshed, contributes the most summer  
272 precipitation of  $19.38 \text{ mm mon}^{-1}$  and occupies 76.06 % of the tracked precipitation  
273 averagely. While the east region, which is in an unfavorable downwind position in the  
274 summer circulation, provides only  $2.81 \text{ mm mon}^{-1}$  summer precipitation, accounting  
275 for 10.68 %.

276 The difference in moisture contribution obtained from the 1998-2019 period minus  
277 the 1980-1997 period is shown in Fig. 4(b). Almost all grid contributions show a  
278 decrease after 1997. The grids with a large moisture contribution decline are mainly  
279 concentrated in the IP, with the maximum reduction exceeding an average of  $3 \text{ mm}$   
280  $\text{mon}^{-1}$  (more than 50% of its climatological moisture contribution). Compared with  
281 other non-local source grids, the grids with higher contributions along the east coast of  
282 the North Atlantic near the IP also have a slight but significant reduction in contribution.

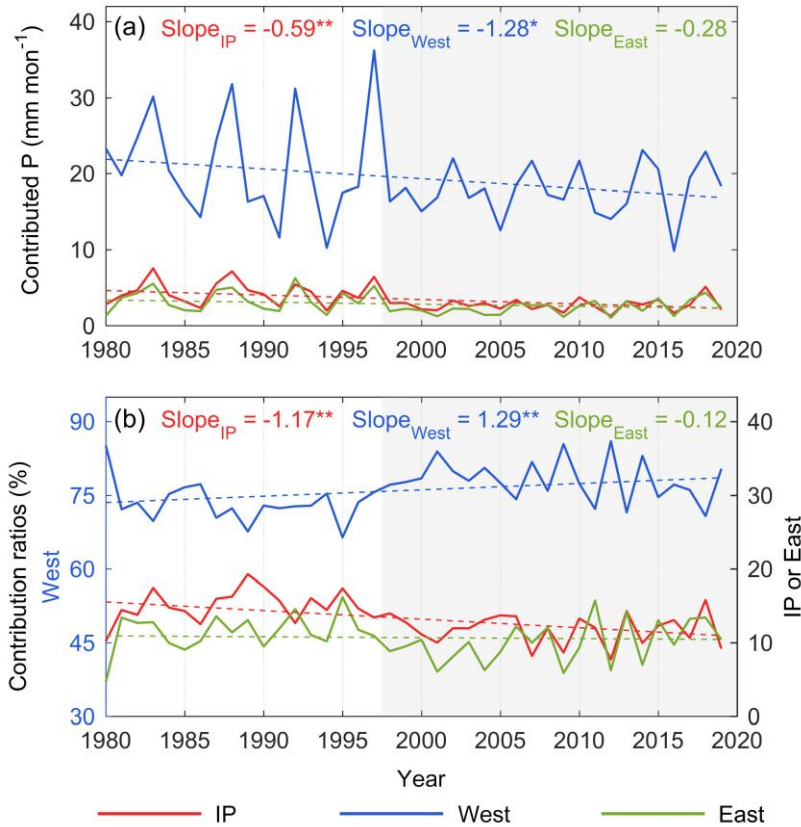
283 Due to the uneven distribution of grid contribution reduction in space, the area of  
284 different percentile precipitationsheds differs in the two periods. The areas with  
285 different colors in the distribution map of Fig. 5 represent the precipitationshed  
286 boundaries at different percentiles in the two periods. During 1998-2019, the  
287 precipitationshed boundary of each percentile extends westward in varying degrees  
288 compared with those before 1997. The top decile of the contribution is still in the  
289 western half of the IP. In the North Atlantic, the westward expansion of the western

290 boundary of the precipitationsheds is conspicuous, especially the 45th and 60th  
 291 percentile precipitationsheds shown in orange and green color in Fig. 5(a, b). This  
 292 westward extension implies that the significant and substantial reduction in the  
 293 contribution of the local grids and its surrounding grids results in a decrease in the  
 294 proportion of these areas. Therefore, for the same percentile of the precipitationshed,  
 295 only a smaller area concentrated by high-contribution grids is sufficient before 1997.  
 296 However, a larger area is required for the same proportion after 1997.



297  
 298 **Figure 5** Different percentile precipitationsheds during the two periods (a) 1980-1997 and (b) 1998-  
 299 2019. The proportion of the cumulative contribution to the IP precipitation from all areas enclosed  
 300 by the contour line is the percentile indicated by the corresponding color.

301 Figure 6(a) shows the quantified precipitation contributed by the local IP, the west  
302 and the east regions. The negative slopes in Fig. 6(a) indicate that the summer  
303 precipitation contributed by these three regions has a downward trend, especially  
304 significant for the IP and the west with slopes of  $-0.59$  and  $-1.28 \text{ mm mon}^{-1} \text{ decade}^{-1}$ .  
305 These decreasing trends cause a  $6.38 \text{ mm mon}^{-1}$  difference in precipitation from the  
306 main source region in the two periods, which explains  $82.64 \%$  of the total reduction in  
307 the IP summer precipitation ( $7.72 \text{ mm mon}^{-1}$ ). In terms of the difference in the average  
308 values of each region, the precipitation contributed by the local IP, the west and the east  
309 significantly decreases from  $4.38$ ,  $21.37$  and  $3.41 \text{ mm mon}^{-1}$  in 1980-1997 to  $2.71$ ,  
310  $17.76$  and  $2.32 \text{ mm mon}^{-1}$  in 1998-2019, respectively.  $26.32 \%$ ,  $56.53 \%$  and  $17.15 \%$   
311 of the difference in the main source supply between the two periods are due to the  
312 contribution decline from the local IP, the west and the east, respectively.



313

314 **Figure 6** Variations of (a) contributed precipitation (unit of the slope: mm mon<sup>-1</sup> decade<sup>-1</sup>) and (b)

315 contribution ratios (unit of the slope: % decade<sup>-1</sup>) from the IP, the west and the east region during

316 1980-2019 summer. ‘\*\*\*’ and ‘\*\*’ represent 0.05 and 0.1 level significance of the trend.

317 The variation and trend of the contribution ratio of each region are shown in Fig.

318 6(b). The proportion of contributions from the local IP and the east shows a decreasing

319 trend throughout the 40 years with the slope of -1.17 % decade<sup>-1</sup> and -0.12 % decade<sup>-1</sup>,

320 which is consistent with the decreasing trends of their absolute contributions.

321 Conversely, although the precipitation contributed by the west shows a decreasing trend,

322 its proportion is significantly increasing and the slope is 1.29 % decade<sup>-1</sup>. The average

323 contribution ratios of the local IP and the east decrease from 15.05 % and 11.49 %

324 before 1997 to 11.79 % and 10.02 % after 1997, while the ratio of the west increases

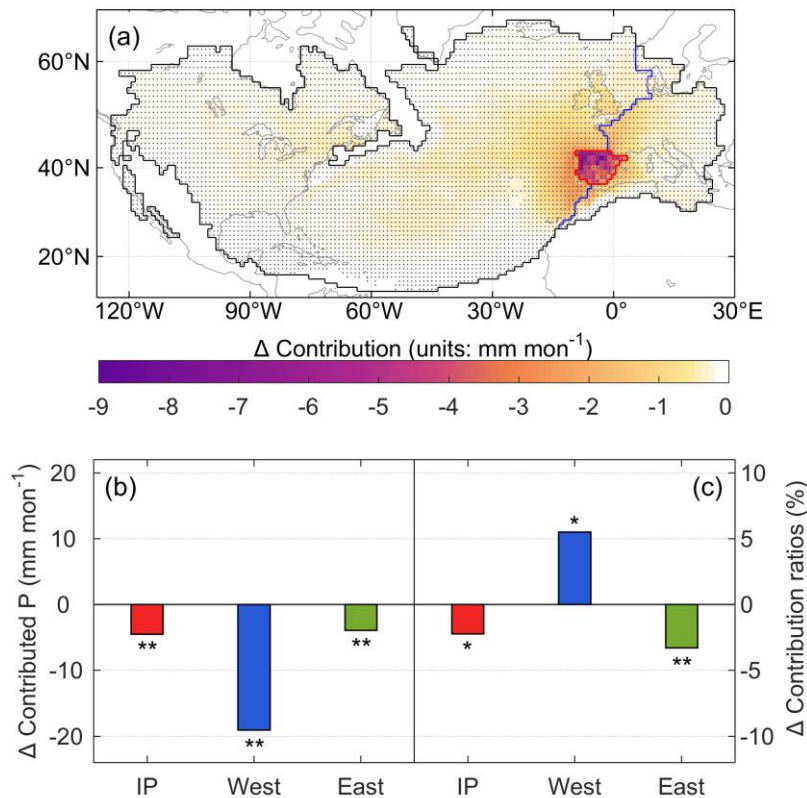
325 from 73.46 % to 78.19 %.

### 326 3.3 Differences in wet years and dry years

327 The dry years (1991, 1994, 2005, 2012 and 2016) and the wet years (1983 1987  
328 1988 1992 and 1997) are selected as described in section 3.1. Of the two divided periods,  
329 all the wet years only occur before 1997, while the dry years are distributed in both  
330 periods with no decrease in its average value. This represents that although the average  
331 summer precipitation after 1997 is reduced significantly compared with the previous  
332 period, there is no decrease in the valley value of the precipitation series. Thus, the  
333 disappearance of the wet years during 1998-2019 caused by the decrease of the  
334 precipitation series peaks directly reflects the recent decrease in the IP summer  
335 precipitation.

336 During the entire 40 years, differences in moisture contribution within the 90<sup>th</sup>  
337 precipitation shed of the IP summer precipitation between the wet and dry years are  
338 shown in Fig. 7(a). In the dry years, the significant reduction in the moisture  
339 contribution from all grids in the main source region induces much lower precipitation  
340 than in the wet years. On the grid scale, the larger declines primarily happened in the  
341 local IP, and the grids with the largest drop, close to 9 mm mon<sup>-1</sup>, are mainly  
342 concentrated in the west and the north of the IP. In each source region, an average of  
343 6.41, 30.74 and 5.34 mm mon<sup>-1</sup> of the summer IP precipitation is provided from the  
344 local IP, the west and the east in the wet years, with 15.15 % recycling ratio, 72.19 %

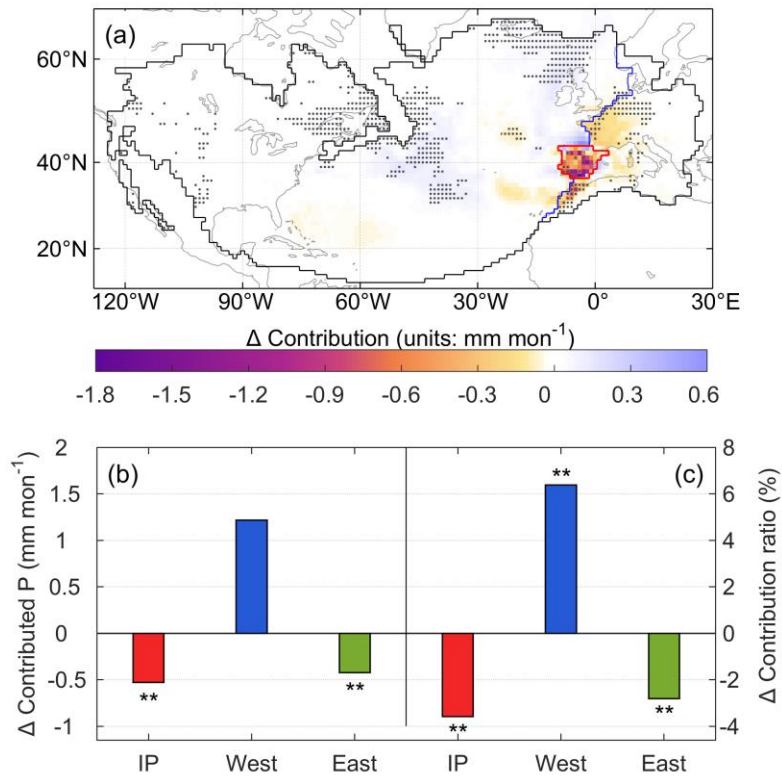
345 and 12.66 % contribution ratio. While in the dry years, the average precipitation  
 346 contributed from each region is 1.92, 11.66 and 1.40 mm mon<sup>-1</sup>, accounting for 12.93 %,  
 347 77.70 % and 9.37 %, respectively. All three regions contribute more to summer  
 348 precipitation in the wet years than in the dry years, and compared with the dry years,  
 349 the contribution ratios of the local IP and the east in the wet years are also higher. The  
 350 disappearance of the wet years after 1997, compared with those before 1997,  
 351 exacerbates the decline in contributions from all three sources, due to the high moisture  
 352 supply in the wet years. The decrease in the frequency of the wet years with higher local  
 353 moisture recycling ratio and higher contribution ratio of the east leads to an increase in  
 354 the proportion of the summer precipitation originating from the remaining other region,  
 355 namely the west, during the same period.



356

357 **Figure 7** (a) Differences in the moisture contribution in the 90<sup>th</sup> precipitation shed between the dry  
358 years and the wet years (average of the dry years minus average of the wet years). The dots indicate  
359 0.1 significance of the difference. The changes in (b) average precipitation contributed from each  
360 region and (c) their average contribution ratios between the dry years and the wet years. ‘\*\*\*’ and ‘\*’  
361 represent 0.05 and 0.1 level significance of the difference.

362 The dry years in the two periods have been divided and compared with each other,  
363 and the differences between the two periods are shown in Fig. 8. From the distribution  
364 of differences, the grids with reduced moisture contribution are mainly located in the  
365 IP and the east region, and the southern part of the IP has the largest decrease (Fig. 8(a)).  
366 Mainly dominated by these negatively changing grids, both the absolute contribution  
367 and the contribution ratio of the local IP and the east have dropped significantly, with  
368 0.53 and 0.42 mm mon<sup>-1</sup> decrease in contributed precipitation and 3.58 % and 2.81 %  
369 contribution ratio reduction, respectively (Fig. 8(b, c)). For the west region, however,  
370 it raises the moisture contribution to the summer precipitation by 1.22 mm mon<sup>-1</sup> in the  
371 dry years after 1997, causing a 6.39 % increase in its contribution ratio. Despite the dry  
372 years with no decrease precipitation between the two periods, the decrease in the local  
373 moisture recycling is still noticeable.



374

375 **Figure 8** (a) Differences in the moisture contribution in the 90<sup>th</sup> precipitation shed in the dry years  
 376 between 1998-2019 and 1980-1997 (average of 1998-2019 minus average of 1980-1997). The dots  
 377 indicate 0.1 significance of the difference. The changes in (b) average precipitation contributed from  
 378 each region and (c) their average contribution ratios in the dry years between 1998-2019 and 1980-  
 379 1997. ‘\*\*\*’ and ‘\*\*’ represent 0.05 and 0.1 level significance of the difference.

#### 380 4. Discussion

381 The trends in the contribution from the three source regions, the local, the west  
 382 and the east regions, to all seasonal and annual precipitation over the past 40 years are  
 383 listed in Table 1. In general, the decreasing trend maintained by the local IP and the east  
 384 region are closely related to the drought in the Mediterranean basin (Ribeiro et al., 2020;  
 385 Russo et al., 2019), and the increasing proportion of the west can be explained by the



386 increasingly important role of the oceanic moisture in terrestrial precipitation (Gimeno  
387 et al., 2020; Vicente-Serrano et al., 2018). The simultaneous decrease in the moisture  
388 contribution from all three regions is responsible for the significant decrease in only the  
389 summer precipitation series among all seasonal or annual precipitation. In particular,  
390 the local moisture recycling ratio in summer is obviously way down, differentiating the  
391 reduced summer precipitation from the other seasons. It is worth highlighting that this  
392 significant decrease in recent summer precipitation over the IP in this study is based on  
393 a short record (1980-2019) from ERA5, while a long-term assessment of precipitation  
394 (1850-2018) from multiple sources still lacks a statistically significant decreasing trend  
395 (Peña-Angulo et al., 2020). Nevertheless, the changes in the recent four decades still  
396 show the significant influence of the local moisture recycling, especially on the trend  
397 of summer precipitation and variation of summer wet and dry years.

398

399 **Table 1** Trends of contributions from the IP, the west and the east to annual and seasonal  
400 precipitation, and the trends of their contribution ratios.

	Contributed precipitation (mm mon <sup>-1</sup> decade <sup>-1</sup> )					Contribution ratio (% decade <sup>-1</sup> )				
	Annual	Spring	Summer	Autumn	Winter	Annual	Spring	Summer	Autumn	Winter
IP	-0.24**	-0.30	-0.59**	-0.03	-0.03	-0.49**	-0.66**	-1.17**	-0.14	-0.08
West	0.53	1.67	-1.28*	1.23	0.52	0.81**	0.80	1.29**	0.38	0.77
East	-0.17	-0.06	-0.28	-0.05	-0.29	-0.32	-0.14	-0.12	-0.24	-0.69

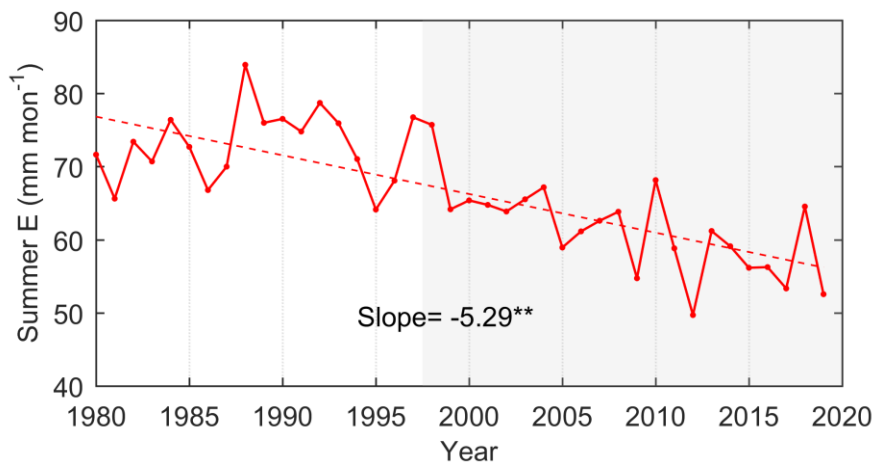
401 ‘\*\*’ and ‘\*’ represent 0.05 and 0.1 level significance of the trend.

402 The remarkable decrement of summer precipitation can be attributed to the

403 simultaneous and large reduction of contributions from all three source regions.  
404 Moisture transport from the west region contributing to the IP precipitation is mainly  
405 through the tropical–subtropical North Atlantic corridor. In summer, air masses from  
406 the west in this transportation process, as it gets closer to the destination, gradually shift  
407 from a net supply to a net uptake of the IP precipitation (Gimeno et al., 2010). In this  
408 case, the stronger land-sea contrast caused by the warming land surface makes the  
409 advected air mass from the Atlantic experience more drying and a decrease in the  
410 contribution from the west (Cramer et al., 2018; Kröner et al., 2017). In addition, the  
411 extension of Hadley circulation makes the IP more strongly affected by subsidence,  
412 generating higher static stability (Brogli et al., 2019). This results in a lower frequency  
413 of extreme heavy precipitation characterized by the presence of a cutoff low at mid-  
414 levels and an easterly moisture flow from the Mediterranean Sea (Merino et al., 2016).  
415 However, the ocean warming patterns and thermodynamics can promote precipitation  
416 in cold seasons (Brogli et al., 2019), just as shown by the increasing contributed  
417 precipitation from the west in autumn and winter in Table 1. It suggests the drivers  
418 leading to less summer precipitation do not generally cause a similar change in the  
419 precipitation in the other seasons.

420 In terms of the total contribution from the three subregions, the west region  
421 dominates more of the reduction in the IP precipitation due to its wide coverage with a  
422 large number of grids. Nevertheless, in the local IP, which is much smaller than the  
423 west, the high contribution per grid, the difference between the two periods, and the

424 consistent decline of the precipitation recycling ratio make the role of the local  
425 contribution variation worth emphasizing. As an important indicator to describe the  
426 interaction between the surface and atmospheric processes, the change in the  
427 precipitation recycling ratio takes into account changes in both precipitation and the  
428 contribution of local evaporation (Goessling and Reick, 2011; Zhang, 2020). For the IP,  
429 its significant reduction in local moisture contribution is most likely due to the  
430 weakening of local evaporation (Fig. 9), with a correlation coefficient of 0.64 between  
431 evaporation and the locally contributed precipitation. In summer, soil moisture and the  
432 recycling process driven by evaporation are regarded as an active source of moisture  
433 (Jung et al., 2010; Vicente-Serrano et al., 2014), leading to a positive correlation  
434 between soil moisture and precipitation. As a result, during those dry summers, the  
435 declining precipitation causes the shortage of soil water supply, the limitation of soil  
436 water evaporation capacity and the consequent reduction in surface evaporation  
437 (García-Valdecasas Ojeda et al., 2020; Ruosteenoja et al., 2018). The IP precipitation  
438 can be further reduced due to this weakening of the local moisture recycling. This  
439 continuous feedback of the interactions of soil moisture evaporation and precipitation  
440 can exacerbate the water resource depletion and summer drought, especially in dry  
441 years. Thus, despite the ongoing emphasis on the significance of the ocean as a moisture  
442 source, consistent changes in the local moisture contribution or proportion with reduced  
443 precipitation require more attention.



444

445 **Figure 9** Time series of the IP summer evaporation from the ERA5 during 1980-2019 (unit of the  
 446 slope: mm mon<sup>-1</sup> decade<sup>-1</sup>). ‘\*\*\*’ represents 0.05 level significance of the trend.

## 447 5. Conclusions

448 Decreasing summer precipitation over the IP could lead to an escalation of drought,  
 449 especially with the high temperature and low rainfall characteristics of Mediterranean  
 450 climate. In this study, using the reanalysis data ERA5 and WAM-2layers model, we  
 451 investigated how changes in moisture contribution from the sources, including the IP,  
 452 the west and the east, affect the reduction in summer precipitation between 1980-1997  
 453 and 1998-2019. The major findings attribute the decreasing precipitation to the changes  
 454 in moisture contribution at sources and highlight their importance, which are  
 455 summarized below.

456 1) The reduction of contribution to IP summer precipitation is mainly concentrated in  
 457 the IP and its neighboring grids. The local IP grids show the greatest reduction, and  
 458 the surrounding grids show a slight but significant decrease.

459 2) Compared with the summer of 1980-1997, the IP and the east contributed 1.7 and

460 1.1 mm mon<sup>-1</sup> less IP precipitation during 1998-2019, accounting for 26% and 17%  
461 of the main source supply reduction, respectively. Meanwhile, the importance of  
462 the vast west region was clearly shown by reducing the IP precipitation by 3.6 mm  
463 mon<sup>-1</sup>, representing 57% of the decrease in precipitation originating from main  
464 sources.

465 3) The contributions from the local IP and the east keep declining during the 40 years.  
466 In particular, the significant reduction in the local moisture recycling, reflected in  
467 the disappearance of the wet years after 1997 and the reduction of local  
468 contributions in the dry years, suggests a close link with the decrease in summer  
469 precipitation.

470

#### 471 **Code and Data availability**

472 Code and data used in this manuscript are available from the corresponding author upon  
473 a reasonable request.

474

#### 475 **Author contributions**

476 MG and QT designed the study; YL performed the analysis and calculation; CZ  
477 contributed to the application of the model in this study; YL prepared the manuscript  
478 draft, and all co-authors reviewed and edited the manuscript.

479

#### 480 **Competing interests**

481 The authors declare no competing interests.

482

483 **Acknowledgements**

484 This study was partly funded by the National Natural Science Foundation of China

485 (41730645 and 41701033) and the Strategic Priority Research Program of Chinese

486 Academy of Sciences (XDA20060402). The authors would like to thank the EU and

487 Innovation Fund Denmark (IFD) for funding within the framework of the FORWARD

488 collaborative international consortium financed through the ERA-NET co-fund

489 WaterWorks2015 integral part of the 2016 joint activities developed by the “Water

490 Challenges for a Changing World” joint programme initiative (Water JPI).

491

## 492 **References**

- 493 Boé, J., and Terray, L.: Land–sea contrast, soil-atmosphere and cloud-temperature  
494 interactions: interplays and roles in future summer European climate change,  
495 *Clim. Dyn.*, 42, 683-699, <https://doi.org/10.1007/s00382-013-1868-8>, 2014.
- 496 Boé, J., Terray, L., Cassou, C., and Najac, J.: Uncertainties in European summer  
497 precipitation changes: role of large scale circulation, *Clim. Dyn.*, 33, 265-276,  
498 <https://doi.org/10.1007/s00382-008-0474-7>, 2009.
- 499 Bonne, J. L., Masson-Delmotte, V., Cattani, O., Delmotte, M., and Steen-Larsen, H. C.:  
500 The isotopic composition of water vapour and precipitation in Ivittuut, Southern  
501 Greenland, *Atmos. Chem. Phys.*, 14, 4419-2014, <https://doi.org/10.5194/acp-14-4419-2014>, 2014.
- 503 Brogli, R., Sørland, S. L., Kröner, N., and Schär, C.: Causes of future Mediterranean  
504 precipitation decline depend on the season, *Environ. Res. Lett.*, 14, 114017,  
505 <https://doi.org/10.1088/1748-9326/ab4438>, 2019.
- 506 Burde, G. I.: Bulk recycling models with incomplete vertical mixing. Part I: Conceptual  
507 framework and models, *J. Clim.*, 19, 1461-1472,  
508 <https://doi.org/10.1175/jcli3687.1>, 2010.
- 509 Cortesi, N., Trigo, R. M., Gonzalez-Hidalgo, J. C., and Ramos, A. M.: Modeling  
510 monthly precipitation with circulation weather types for a dense network of  
511 stations over Iberia, *Hydrol. Earth Syst. Sci.*, 17, 665-678,  
512 <https://doi.org/10.5194/hess-17-665-2013>, 2013.
- 513 Cramer, W., Guiot, J., Fader, M., Garrabou, J., Gattuso, J.-P., Iglesias, A., . . . Xoplaki,  
514 E.: Climate change and interconnected risks to sustainable development in the  
515 Mediterranean, *Nat. Clim. Chang.*, 8, 972-980, <https://doi.org/10.1038/s41558-018-0299-2>, 2018.
- 517 Damián, I.-C., and Gonzalo, M. M.: A new moisture tagging capability in the Weather  
518 Research and Forecasting model: formulation, validation and application to the  
519 2014 Great Lake-effect snowstorm, *Earth Syst. Dynam.*, 9, 167-185,  
520 <https://doi.org/10.5194/esd-9-167-2018>, 2018.
- 521 García-Valdecasas Ojeda, M., Yeste, P., Gámiz-Fortis, S. R., Castro-Díez, Y., and  
522 Esteban-Parra, M. J.: Future changes in land and atmospheric variables: An  
523 analysis of their couplings in the Iberian Peninsula, *Sci. Total Environ.*, 722,  
524 137902, <https://doi.org/10.1016/j.scitotenv.2020.137902>, 2020.
- 525 Gimeno, L., Nieto, R., and Sorí, R.: The growing importance of oceanic moisture  
526 sources for continental precipitation, *npj Clim. Atmos. Sci.*, 3, 27,  
527 <https://doi.org/10.1038/s41612-020-00133-y>, 2020.
- 528 Gimeno, L., Nieto, R., Trigo, R. M., Vicente-Serrano, S. M., and López-Moreno, J. I.:  
529 Where does the Iberian Peninsula moisture come from? An answer based on a  
530 Lagrangian approach, *J. Hydrometeorol.*, 11, 421-436,  
531 <https://doi.org/10.1175/2009JHM1182.1>, 2010.

532 Goessling, H. F., and Reick, C. H.: What do moisture recycling estimates tell us?  
533 Exploring the extreme case of non-evaporating continents, *Hydrol. Earth Syst.*  
534 *Sci.*, 15, 3217-3235, <https://doi.org/10.5194/hess-15-3217-2011>, 2011.

535 Goessling, H. F., and Reick, C. H.: On the "well-mixed" assumption and numerical 2-  
536 D tracing of atmospheric moisture, *Atmos. Chem. Phys.*, 13, 5567-5585,  
537 <https://doi.org/10.5194/acp-13-5567-2013>, 2013.

538 Herrera, S., Cardoso, R. M., Soares, P. M., Espírito-Santo, F., and Gutiérrez, J.: Iberia01:  
539 a new gridded dataset of daily precipitation and temperatures over Iberia, *Earth*  
540 *Syst. Sci. Data*, 11, 1947-1956, <https://doi.org/10.5194/essd-11-1947-2019>,  
541 2019.

542 Hersbach, H., Bell, B., Berrisford, P., Hirahara, S., Horányi, A., Muñoz-Sabater, J., . . .  
543 Thépaut, J.-N.: The ERA5 global reanalysis, *Quarterly Journal of the Royal*  
544 *Meteorological Society*, 146, 1999-2049, <https://doi.org/10.1002/qj.3803>, 2020.

545 Jung, M., Reichstein, M., Ciais, P., Seneviratne, S. I., Sheffield, J., Goulden, M. L., . . .  
546 Zhang, K.: Recent decline in the global land evapotranspiration trend due to  
547 limited moisture supply, *Nature*, 467, 951-954,  
548 <https://doi.org/10.1038/nature09396>, 2010.

549 Keys, P. W., Barnes, E. A., van der Ent, R. J., and Gordon, L. J.: Variability of moisture  
550 recycling using a precipitationshed framework, *Hydrology and Earth System*  
551 *Sciences*, 18, 3937-3950, <https://doi.org/10.5194/hess-18-3937-2014>, 2014.

552 Keys, P. W., Ent, R., Gordon, L. J., Hoff, H., and Savenije, H.: Analyzing  
553 precipitationsheds to understand the vulnerability of rainfall dependent regions,  
554 *Biogeosciences Discussions*, 8, 2011.

555 Kröner, N., Kotlarski, S., Fischer, E., Lüthi, D., Zubler, E., and Schär, C.: Separating  
556 climate change signals into thermodynamic, lapse-rate and circulation effects:  
557 theory and application to the European summer climate, *Clim. Dyn.*, 48, 3425-  
558 3440, <https://doi.org/10.1007/s00382-016-3276-3>, 2017.

559 Lenderink, G., van Ulden, A., van den Hurk, B., and van Meijgaard, E.: Summertime  
560 inter-annual temperature variability in an ensemble of regional model  
561 simulations: analysis of the surface energy budget, *Clim. Change*, 81, 233-247,  
562 <https://doi.org/10.1007/s10584-006-9229-9>, 2007.

563 Lopez-Bustins, J. A., and Lemus-Canovas, M.: The influence of the Western  
564 Mediterranean Oscillation upon the spatio-temporal variability of precipitation  
565 over Catalonia (northeastern of the Iberian Peninsula), *Atmos. Res.*, 236,  
566 104819, <https://doi.org/10.1016/j.atmosres.2019.104819>, 2020.

567 Maasch, K. A.: Statistical detection of the mid-Pleistocene transition, *Climate*  
568 *Dynamics*, 2, 133-143, <https://doi.org/10.1007/BF01053471>, 1988.

569 Merino, A., Fernández-Vaquero, M., López, L., Fernández-González, S., Hermida, L.,  
570 Sánchez, J. L., . . . Gascón, E.: Large-scale patterns of daily precipitation  
571 extremes on the Iberian Peninsula, *International Journal of Climatology*, 36,  
572 3873-3891, <https://doi.org/https://doi.org/10.1002/joc.4601>, 2016.



573 Numaguti, A.: Origin and recycling processes of precipitating water over the Eurasian  
574 continent: Experiments using an atmospheric general circulation model, *J.*  
575 *Geophys. Res.-Atmos.*, 104, 1957-1972,  
576 <https://doi.org/10.1029/1998JD200026>, 1999.

577 Páscoa, P., Russo, A., Gouveia, C. M., Soares, P. M. M., Cardoso, R. M., Careto, J. A.  
578 M., and Ribeiro, A. F. S.: A high-resolution view of the recent drought trends  
579 over the Iberian Peninsula, *Weather Clim. Extremes*, 32, 100320,  
580 <https://doi.org/10.1016/j.wace.2021.100320>, 2021.

581 Peña-Angulo, D., Vicente-Serrano, S. M., Domínguez-Castro, F., Murphy, C., Reig, F.,  
582 Trambly, Y., . . . El Kenawy, A.: Long-term precipitation in Southwestern  
583 Europe reveals no clear trend attributable to anthropogenic forcing, *Environ.*  
584 *Res. Lett.*, 15, 094070, <https://doi.org/10.1088/1748-9326/ab9c4f>, 2020.

585 Rajczak, J., and Schär, C.: Projections of future precipitation extremes over Europe: A  
586 multimodel assessment of climate simulations, *J. Geophys. Res.-Atmos.*, 122,  
587 10,773-710,800, <https://doi.org/10.1002/2017JD027176>, 2017.

588 Ribeiro, A. F. S., Russo, A., Gouveia, C. M., and Pires, C. A. L.: Drought-related hot  
589 summers: A joint probability analysis in the Iberian Peninsula, *Weather Clim.*  
590 *Extremes*, 30, 100279, <https://doi.org/10.1016/j.wace.2020.100279>, 2020.

591 Ruosteenoja, K., Markkanen, T., Venäläinen, A., Räisänen, P., and Peltola, H.: Seasonal  
592 soil moisture and drought occurrence in Europe in CMIP5 projections for the  
593 21st century, *Clim. Dyn.*, 50, 1177-1192, [https://doi.org/10.1007/s00382-017-](https://doi.org/10.1007/s00382-017-3671-4)  
594 [3671-4](https://doi.org/10.1007/s00382-017-3671-4), 2018.

595 Russo, A., Gouveia, C. M., Dutra, E., Soares, P. M. M., and Trigo, R. M.: The synergy  
596 between drought and extremely hot summers in the Mediterranean, *Environ.*  
597 *Res. Lett.*, 14, 014011, <https://doi.org/10.1088/1748-9326/aaf09e>, 2019.

598 Serrano, A., García, J. A., Mateos, V. L., Cancillo, M. L., and Garrido, J.: Monthly  
599 modes of variation of precipitation over the Iberian Peninsula, *J. Clim.*, 12,  
600 2894-2919, 1999.

601 Stohl, A., and James, P.: A Lagrangian analysis of the atmospheric branch of the global  
602 water cycle. Part I: Method description, validation, and demonstration for the  
603 August 2002 flooding in Central Europe, *J. Hydrometeorol.*, 5, 656, 2004.

604 Stohl, A., and James, P.: A Lagrangian analysis of the atmospheric branch of the global  
605 water cycle. Part II: Moisture transports between earth's ocean basins and river  
606 catchments, *J. Hydrometeorol.*, 6, 961-984, <https://doi.org/10.1175/JHM470.1>,  
607 2005.

608 Tang, Q., Leng, G., and Groisman, P. Y.: European hot summers associated with a  
609 reduction of cloudiness, *J. Clim.*, 25, 3637-3644, [https://doi.org/10.1175/JCLI-](https://doi.org/10.1175/JCLI-D-12-00040.1)  
610 [D-12-00040.1](https://doi.org/10.1175/JCLI-D-12-00040.1), 2012.

611 Teuling, A. J., Van Loon, A. F., Seneviratne, S. I., Lehner, I., Aubinet, M., Heinesch,  
612 B., . . . Spank, U.: Evapotranspiration amplifies European summer drought,  
613 *Geophys. Res. Lett.*, 40, 2071-2075, <https://doi.org/10.1002/grl.50495>, 2013.

614 Ulbrich, U., Christoph, M., Pinto, J. G., and Corte-Real, J.: Dependence of winter  
615 precipitation over Portugal on NAO and baroclinic wave activity, *International*  
616 *Journal of Climatology*, 19, 379-390, [https://doi.org/10.1002/\(SICI\)1097-0088\(19990330\)19:4<379::AID-JOC357>3.0.CO;2-8](https://doi.org/10.1002/(SICI)1097-0088(19990330)19:4<379::AID-JOC357>3.0.CO;2-8), 2015.

618 van der Ent, R. J., and Savenije, H. H. G.: Length and time scales of atmospheric  
619 moisture recycling, *Atmos. Chem. Phys.*, 11, 1853-1863,  
620 <https://doi.org/10.5194/acp-11-1853-2011>, 2011.

621 van der Ent, R. J., Savenije, H. H. G., Schaeffli, B., and Steele-Dunne, S. C.: Origin and  
622 fate of atmospheric moisture over continents, *Water Resour. Res.*, 46,  
623 <https://doi.org/10.1029/2010WR009127>, 2010.

624 van der Ent, R. J., Tuinenburg, O. A., Knoche, H. R., Kunstmann, H., and Savenije, H.  
625 H. G.: Should we use a simple or complex model for moisture recycling and  
626 atmospheric moisture tracking?, *Hydrol. Earth Syst. Sci.*, 17, 4869-4884,  
627 <https://doi.org/10.5194/hess-17-4869-2013>, 2013.

628 van der Ent, R. J., Wang-Erlandsson, L., Keys, P., and Savenije, H.: Contrasting roles  
629 of interception and transpiration in the hydrological cycle - Part 2: Moisture  
630 recycling, *Earth Syst. Dynam.*, 5, <https://doi.org/10.5194/esdd-5-281-2014>,  
631 2014.

632 Vázquez, M., Nieto, R., Liberato, M. L. R., and Gimeno, L.: Atmospheric moisture  
633 sources associated with extreme precipitation during the peak precipitation  
634 month, *Weather and Climate Extremes*, 30, 100289,  
635 <https://doi.org/https://doi.org/10.1016/j.wace.2020.100289>, 2020.

636 Vicente-Serrano, S. M., Azorin-Molina, C., Sanchez-Lorenzo, A., Morán-Tejeda, E.,  
637 Lorenzo-Lacruz, J., Revuelto, J., . . . Espejo, F.: Temporal evolution of surface  
638 humidity in Spain: recent trends and possible physical mechanisms, *Clim. Dyn.*,  
639 42, 2655-2674, <https://doi.org/10.1007/s00382-013-1885-7>, 2014.

640 Vicente-Serrano, S. M., Nieto, R., Gimeno, L., Azorin-Molina, C., Drumond, A., El  
641 Kenawy, A., . . . Peña-Gallardo, M.: Recent changes of relative humidity:  
642 regional connections with land and ocean processes, *Earth Syst. Dynam.*, 9,  
643 915-937, <https://doi.org/10.5194/esd-9-915-2018>, 2018.

644 Zhang, C.: Moisture source assessment and the varying characteristics for the Tibetan  
645 Plateau precipitation using TRMM, *Environ. Res. Lett.*, 15, 104003,  
646 <https://doi.org/10.1088/1748-9326/abac78>, 2020.

647 Zhang, C., Tang, Q., and Chen, D.: Recent changes in the moisture source of  
648 precipitation over the Tibetan Plateau, *J. Clim.*, 30, 1807-1819,  
649 <https://doi.org/10.1175/JCLI-D-15-0842.1>, 2017.

650 Zhang, Y., Huang, W., Zhang, M., Tian, Y., Wang, G., and Zhong, D.: Atmospheric  
651 Basins: Identification of Quasi-Independent Spatial Patterns in the Global  
652 Atmospheric Hydrological Cycle Via a Complex Network Approach, *J.*  
653 *Geophys. Res.-Atmos.*, 125, e2020JD032796,  
654 <https://doi.org/https://doi.org/10.1029/2020JD032796>, 2020.

655 Zhu, Y., and Newell, R. E.: A proposed algorithm for moisture fluxes from atmospheric  
656 rivers, Mon. Weather Rev., 126, 725-735, [https://doi.org/10.1175/1520-  
657 0493\(1998\)126<0725:Apafmf>2.0.Co;2](https://doi.org/10.1175/1520-0493(1998)126<0725:Apafmf>2.0.Co;2), 1998.  
658